Editors' Suggestion | Featured in Physics

Emergent Fine Structure Constant of Quantum Spin Ice Is Large

Salvatore D. Pace,[1,2] Siddhardh C. Morampudi,[3] Roderich Moessner,[4] and Chris R. Laumann[2]
[1]TCM Group, Cavendish Laboratory, University of Cambridge, Cambridge CB3 0HE, United Kingdom
[2]Department of Physics, Boston University, Boston, Massachusetts 02215, USA
[3]Center for Theoretical Physics, Massachusetts Institute of Technology, Cambridge, Massachusetts 02139, USA
[4]Max-Planck-Institut für Physik komplexer Systeme, 01187 Dresden, Germany

(Received 6 May 2021; accepted 30 July 2021; published 9 September 2021)

Condensed-matter systems provide alternative "vacua" exhibiting emergent low-energy properties drastically different from those of the standard model. A case in point is the emergent quantum electrodynamics (QED) in the fractionalized topological magnet known as quantum spin ice, whose magnetic monopoles set it apart from the familiar QED of the world we live in. Here, we show that the two greatly differ in their fine structure constant α, which parametrizes how strongly matter couples to light: α_{QSI} is more than an order of magnitude greater than $\alpha_{\mathrm{QED}} \approx 1/137$. Furthermore, α_{QSI}, the emergent speed of light, and all other parameters of the emergent QED, are tunable by engineering the microscopic Hamiltonian. We find that α_{QSI} can be tuned all the way from zero up to what is believed to be the strongest possible coupling beyond which QED confines. In view of the small size of its constrained Hilbert space, this marks out quantum spin ice as an ideal platform for studying exotic quantum field theories and a target for quantum simulation. The large α_{QSI} implies that experiments probing candidate condensed-matter realizations of quantum spin ice should expect to observe phenomena arising due to strong interactions.

DOI: 10.1103/PhysRevLett.127.117205

The fine structure constant of QED, $\alpha_{\mathrm{QED}} \approx 1/137$, is famously measurable in a semiconductor device [1], oblivious to any imperfections of the crystal, and perfectly immutable compared to measurements *in vacuo* [2]. By contrast, a fine structure constant is also known to emerge entirely independently in quantum condensed-matter phases whose emergent excitations mimic QED [3,4]. This emergent fine structure constant has no reason to be as constrained as that in QED and this allows emergent QEDs (eQED) to probe physical regimes which are usually difficult to access either theoretically or experimentally.

Among the various microscopic models which host an eQED [3,5–8], the ones which have received the most attention recently in experiments go under the name of quantum spin ice [9–13]. The term quantum spin ice (QSI) simultaneously refers to a family of models, as well as a class of rare-earth magnetic materials which approximately realize the theoretical models. Similar to the prototypical gauge theory of QED which has matter excitations such as electrons and a gauge boson corresponding to the photon, the eQED in QSI is a $3+1$D compact $U(1)$ gauge theory and has "matter" excitations [14]—electric charges [which are the spinons shown in Fig. 1(a)] and magnetic monopoles—and an (emergent) photon [8,15]. These emergent photons and spinons have been established by various theoretical and numerical studies [16–19], with the magnetic monopoles being the focus of recent studies [20,21]. Understanding the properties of the eQED necessitates not just identification of the low-energy emergent excitations, but also measuring the various couplings of the eQED such as the speed of light c_{QSI}. These can be drastically different from those of usual QED, giving access to unusual regimes and phenomenology typically inaccessible in our world. For example, estimates of c_{QSI} are quite small [8,11,18]. This means that experiments can probe phenomena ranging from the nonrelativistic to the ultrarelativistic, where the electric charges move faster than the speed of light and emit Cerenkov radiation.

However, there is currently no estimate of the electric charge e_{QSI} and hence fine structure constant $\alpha_{\mathrm{QSI}} \equiv e_{\mathrm{QSI}}^2/\hbar c_{\mathrm{QSI}}$ (in fact, in any microscopic model with an eQED). This dimensionless quantity characterizes how strongly the spinons (which are the electric charges of the theory) interact with the emergent photon [see Fig. 1(b)]. In usual QED, the small value of α_{QED} justifies a perturbative treatment, while also making some processes like photon-photon scattering very difficult to observe. Determining the value of α_{QSI} would allow us to guide theoretical treatments of its eQED and also potentially place the eQED in a different regime to QED.

Here, we determine the fine structure constant α_{QSI} in the eQED of QSI. Besides being an order of magnitude larger than α_{QED}, it is *tunable* over the complete theoretical range by adding local interactions to the microscopic Hamiltonian. This also constitutes a clear example where modifying the microscopic details of a theory changes the emergent couplings of the low-energy theory in a straightforward

 © 2021 American Physical Society

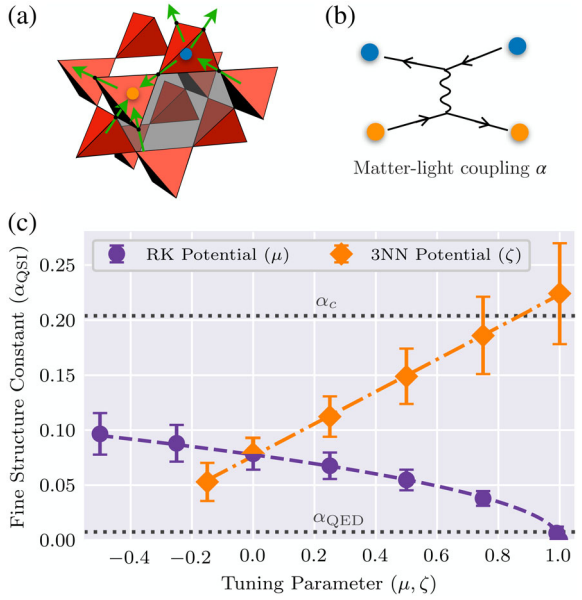

FIG. 1. (a) The pyrochlore lattice of quantum spin ice (QSI) is formed from corner sharing tetrahedra with spin 1/2 s residing at corners. The spins shown give an example of ice-rule violating tetrahedra that correspond to an electric charge-anticharge pair. (b) The emergent electric charges and photons can interact, just as electrons and photons do in QED, and their interaction strength is given by the emergent fine structure constant α_{QSI}. (c) The value of α_{QSI} in the eQED phase of the microscopic QSI Hamiltonian [see Eq. (2)] shown as a function of μ (with $\zeta = 0$) and ζ (with $\mu = 0$). Error bars represent the standard deviation of α_{QSI} among its shape-dependent variations at a fixed (μ, ζ). By varying the 3NN potential, α is tunable up to the maximum value α_c (dotted line) beyond which it is conjectured that any compact QED in 3 + 1D confines [22–24].

manner. Our main results are displayed in Fig. 1(c) and in Table I. From a methodological perspective, the framework we have developed using large-scale exact diagonalization (ED) techniques in constrained spaces may be of additional interest in determining the low-energy properties of other microscopic models with exotic emergent theories.

Microscopics.—Spin ice is modeled by spin-1/2 particles residing on the corners of the tetrahedra of the pyrochlore lattice, shown in Fig. 1(a) [9]. Each spin is restricted to point either toward or away from the centers of the two adjacent tetrahedra. With this restriction, the classical ground state follows a simple rule [25]: each tetrahedron has two spins pointing in and two pointing out. This "2-in 2-out" local constraint is called the ice rule, named after a similar constraint in water ice [26]. Classical spin ice is well understood in terms of fractionalized spins forming an emergent classical electromagnetism, with the ice rule playing the role of Gauss's law. Local violations of the ice rule then correspond to spinons and antispinons [27], which we refer to as electric charges and anticharges. At low temperatures, quantum fluctuations allow tunneling between classical configurations satisfying the ice rule,

TABLE I. Numerical values of the fine structure constant $\alpha = e^2/\hbar c$, the speed of light c, the elementary electric charge e, and the elementary magnetic charge from Dirac quantization $m = e/2\alpha$. In our units, the electric (magnetic) charge squared corresponds to the energy between two electric charges (magnetic monopoles) held one nanometer apart. The second column uses characteristic scales obtained from the pyrochlore oxides, corresponding to $\mu = \zeta = 0$, $a = 10$ Å, and $g \sim 1$ μeV. We stress that the dimensionful values of a and g do not affect α_{QSI}. The corresponding values in the vacuum QED of our Universe are shown in the third column.

	Candidate QSI material	Vacuum QED
α	1/10	1/137
c	1 ms^{-1}	3.0×10^8 ms^{-1}
e	10^{-4} $\sqrt{\mathrm{eV\,nm}}$	1.2 $\sqrt{\mathrm{eV\,nm}}$
m	10^{-3} $\sqrt{\mathrm{eV\,nm}}$	82.2 $\sqrt{\mathrm{eV\,nm}}$

giving rise to an eQED [8,16–19,28–31]. In addition to the electric charges, there are now magnetic monopoles as well as photons corresponding to coherent ring-exchange processes within the ice manifold.

The microscopic Hamiltonian to describe QSI materials was derived, and studied in considerable detail, in the context of the rare-earth pyrochlore materials [9,29,32]. For the present purposes, it is sufficient to consider a simplified model given by the canonical QSI Hamiltonian which consists of two parts [8]: a "classical" term enforcing the ice rules, which determines the cost of an electric charge; and a "quantum" resonance term, also known as a loop flip or ring exchange term, $W_{\hexagon}$, which coherently flips a sequence of six spins arranged head to tail around a hexagon $\hexagon \to \hexagon$,

$$H_{\mathrm{eff}} = J_{zz} \sum_{\langle i,j \rangle} S_i^z S_j^z - g \sum_{\hexagon} (W_{\hexagon} + W_{\hexagon}^{\dagger}). \qquad (1)$$

The first sum runs over all bonds of the pyrochlore lattice and the second over all of its hexagonal plaquettes. A hexagonal plaquette on which $W_{\hexagon}$ acts is shaded in Fig. 1(a). This Hamiltonian describes the standard low-energy dynamics of geometrically frustrated systems capturing phenomena ranging from high-temperature superconductivity to frustrated magnetism [33], and can be obtained as a low-energy effective theory of the general microscopic quantum spin ice model [8,30] Furthermore, it can be formally rewritten as a compact $U(1)$ lattice gauge theory [8,17], with $W_{\hexagon}$ the smallest possible Wilson loop.

To effect the above-mentioned tuning, we additionally consider a pair of simple perturbations to H_{eff}:

$$H_p = \zeta \sum_{\langle\langle i,j \rangle\rangle} S_i^z S_j^z + \mu \sum_{\hexagon} (W_{\hexagon}^{\dagger} W_{\hexagon} + W_{\hexagon} W_{\hexagon}^{\dagger}). \qquad (2)$$

The first summation over $\langle\langle\langle i,j\rangle\rangle\rangle$ runs over the third-nearest neighbors (3NN), which are pairs of spins across from each other on a hexagonal plaquette. This two-body Ising term generically exists in material realizations [29] and can be engineered in many current quantum simulators [34–36]. It prefers spins across from each other to be (anti) parallel (depending on the sign of ζ), hence affecting the number of flippable hexagons ( ). The second term is a Rokhsar-Kivelson (RK) potential, which directly counts the number of flippable hexagons and, as a six body term, is less easy to control experimentally. However, the ground state is exactly solvable at the RK point [37] ($\zeta = 0$ and $\mu = 1$) which allows us to validate our numerics by comparing to previous analytic and numerical studies [7,17,18]. We note that tuning either of these perturbations to be sufficiently strong causes the system to transition out of the deconfined QED phase, which we find persists for $-0.5 \lesssim \mu \leq 1$ at $\zeta = 0$ [17], and for $-0.2 \lesssim \zeta \lesssim 1$ at $\mu = 0$ (see Supplemental Material [38]).

Macroscopic eQED.—The low-energy theory of eQED is the familiar Maxwell Hamiltonian

$$H_{\text{Maxwell}} = \frac{1}{8\pi}\int d^3\boldsymbol{x}(|\boldsymbol{E}|^2 + c_{\text{QSI}}^2|\boldsymbol{B}|^2), \tag{3}$$

where $\boldsymbol{B} = \text{curl}\,\boldsymbol{A}$, and $\boldsymbol{E}$ and $\boldsymbol{A}$ are the canonically conjugate electric field and vector potential operators, respectively. Throughout this manuscript, we use units such that the emergent Coulomb energy between two electric charges (magnetic monopoles) is e_{QSI}^2/r (m_{QSI}^2/r). We fit the low-energy spectra of Eq. (1) in the constrained Hilbert space obeying the classical ice rules, using results from Eq. (3) to extract e_{QSI} and c_{QSI}. See Supplemental Material [38] for a detailed account of the ED techniques used to access the spectra of systems with up to 96 spins.

Since electric charges cannot be excited in the constrained Hilbert space, it may appear that e_{QSI} cannot be probed. However, it is possible to have electric field lines looping through the periodic boundaries without violating the ice rules [8,17]. As a gedanken experiment, an elementary unit of the electric field can be created by first exciting an electric charge-anticharge pair, moving the electric charge around the lattice through a periodic boundary, and then annihilating it with the electric anticharge. This leaves behind an elementary unit of electric flux passing through the boundary. As the dynamics of the QSI Hamiltonian preserve the ice rule locally, the Hilbert space decomposes into electric topological sectors $\boldsymbol{\phi} = (\phi_1, \phi_2, \phi_3) \in \mathbb{Z}^3$, where ϕ_i gives the number of elementary units of electric flux through the ith direction.

The electric field created by this procedure is uniform when the lattice is coarse grained. By computing the ground state energy in each electric topological sector, we can thus extract the value of e_{QSI}. As shown in Supplemental Material [38], $\boldsymbol{E}$ can be found using Gauss's law which then gives an expression for the electric field energy density

$$u = e_{\text{QSI}}^2 \frac{2\pi|Q\boldsymbol{\phi}|^2}{a^4}, \tag{4}$$

where a is the lattice constant of the face-centered cubic lattice underlying the pyrochlore lattice and Q is a dimensionless 3×3 matrix characterizing the shape of the periodic volume. The inset of Fig. 2(a) shows the fit of Eq. (4) to the u ED data at $\mu = \zeta = 0$, yielding $e_{\text{QSI}} = 0.20(1)\sqrt{ag}$. The ED data are obtained across a

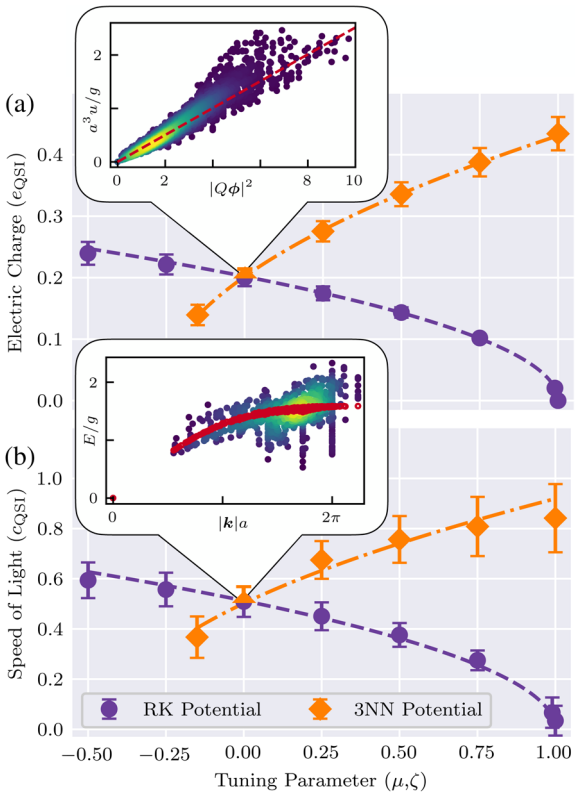

FIG. 2. (a) The emergent electric charge e_{QSI} as a function of RK (μ,$\zeta = 0$) and 3NN ($\mu = 0$, ζ) potential. A representative scatter plot of these data is shown in the inset (data corresponding to $\mu = \zeta = 0$) with associated fit (red line). The dashed lines are fits giving $e_{\text{QSI}} = 0.20\sqrt{ag(1-\mu)}$ at $\zeta = 0$ and $e_{\text{QSI}} = 0.38\sqrt{ag(0.28+\zeta)}$ at $\mu = 0$. We note that the former dependence is predicted near the RK point at $\mu = 1$ [7,17], while the latter is a guide to the eye. (b) The emergent speed of light c_{QSI} as a function of RK and 3NN potential. Representative scatter plot of this dispersion is shown in the inset (at $\mu = \zeta = 0$) with associated fit (red line). Dashed lines are fits giving $c_{\text{QSI}} = 0.51ag\sqrt{1-\mu}/\hbar$ and $c_{\text{QSI}} = 0.78ag\sqrt{0.41+\zeta}/\hbar$ along the $\zeta = 0$ and $\mu = 0$ axes, respectively. Again, we note that the dependence of c on μ near the RK point is consistent with previous results [7,18]. The error bars in both panels represent the standard deviation of e_{QSI} and c_{QSI} among its shape-dependent variations at a fixed (μ, ζ). Furthermore, in both insets, scatter points are brighter the denser their neighboring data points are.

range of finite-size samples (up $N = 96$ spins and 180 different shapes). The spread of the data about the fit, and the corresponding variation in e_{QSI}, comes from the variations in the measurement for different lattice shapes occurring due to the limited sizes accessible with ED.

Figure 2(a) shows e_{QSI} measured at different values of ζ and μ in Eq. (2) along the $\mu = 0$ and $\zeta = 0$ axes, respectively. As ζ becomes increasingly positive and μ increasingly negative, e_{QSI} increases. This has a simple interpretation. Both of these perturbations increase the microscopic energy for spins across hexagonal plaquettes to be parallel, which in terms of the eQED correspond to states with local electric flux in the direction of the parallel spins. This increases the energy of the sectors with global electric flux, producing a larger e_{QSI}.

We measure c_{QSI} using the ground state dispersion of Eq. (1) translated into the first Brillouin zone. At small momenta, one of the photon's key characteristics is its relativistic dispersion $\omega(\boldsymbol{k}) = c_{\mathrm{QSI}}|\boldsymbol{k}|$. The ED data used to extract the fit are obtained across the same range of samples as in the measurement for e_{QSI}. We obtain the value of c_{QSI} by using the Gaussian approximation to the photon dispersion on the pyrochlore (see Supplemental Material [38] for derivation): [18]

$$\omega(\boldsymbol{k}) = \sqrt{\frac{c_{\mathrm{QSI}}^2}{a^2}\lambda(\boldsymbol{k}) + M\lambda^2(\boldsymbol{k})}, \tag{5}$$

where c_{QSI} and M are fitting parameters and $\lambda(\boldsymbol{k}) = 12 - 4\sum_{i>j}\cos(k_i a/2)\cos(k_j a/2)$. The inset of Fig. 2(b) shows the momentum dependence of the ground state energy at $\mu = \zeta = 0$, which upon fitting Eq. (5) gives $c_{\mathrm{QSI}} = 0.51(6)ag/\hbar$. In addition to variation of c_{QSI} coming from lattice shape dependence, there may be spread from the fit due to magnetic monopole states at higher momenta that the Gaussian photon dispersion does not capture [28]; in particular, we exclude $|k|a > \pi$ from the fit, where clear irregularities are visible. We note that the fit value is similar to a previous numerical measurement $c_{\mathrm{QSI}} = 0.6(1)ag/\hbar$ [17] and analytical estimate $c = 0.41ag/\hbar$ [39] using semiclassical techniques.

Using the ED spectra along the μ and ζ axes, Fig. 2(b) shows that like e_{QSI}, c_{QSI} is indeed also tunable. We see a similar trend as previously: c_{QSI} increases as states with a greater number of flippable hexagons become energetically favored. This can be understood qualitatively by noting that the photons are collective motions of fluctuating electric field loops [3]. Since a hexagon has to be flippable to support local electric field loop fluctuations, the photon can propagate to flippable hexagons more rapidly than unflippable ones. At long wavelengths, this corresponds to an increase of the speed of light with increased density of flippable hexagons.

Fine structure constant.—In our units, the fine structure constant is given by $\alpha = e^2/\hbar c$. From our measurements of e_{QSI} and c_{QSI}, upon taking their quotient to find α_{QSI} the dimensionful constants a and g crucially cancel. Figure 1(c) shows α_{QSI} as a function of ζ and μ along the $\mu = 0$ and $\zeta = 0$ axes. Varying μ, we see that α_{QSI} is tunable ranging from exactly zero at the RK point all the way to 0.1 at $\mu = -0.5$, beyond which the system undergoes a first order transition into an ordered state [17]. Along the $\mu = 0$ axis, α_{QSI} is 0.06 at $\zeta = -0.15$ and increases to 0.2 at $\zeta = 1$. At $\zeta \approx 1$, the Hamiltonian undergoes a phase transition into a finite momentum phase, suggesting the development of long-range magnetic order and confinement of the eQED (see Supplemental Material [38]). It is remarkable to note that the value α_{QSI} takes at $\zeta = 1$ corresponds to $\alpha_c \approx 0.2$ at which pure lattice QED on the cubic lattice is known to confine [40]. Indeed, $\alpha_c \approx 0.2$ has been argued to be the limit of stability of the deconfined phase in general [22–24]. Thus, we find that we can tune α_{QSI} over the entire range of fine structure constants allowed by a deconfined QED: $0 \leq \alpha \leq 0.2$.

The dimensionful quantities e_{QSI} and c_{QSI} we have calculated depend on the lattice parameters a and g. There are a large variety of rare-earth pyrochlore oxides that are QSI candidates, such as $Tb_2Ti_2O_7$, $Yb_2Ti_2O_7$, $Pr_2Sn_2O_7$, and $Pr_2Zr_2O_7$ [9,32,41]. The lattice constant in these materials is approximately $a \approx 10$ Å [41] and typical energy values of a candidate QSI material correspond to $g \approx 1$ μeV [29,30]. Using these values, we can estimate e_{QSI} and c_{QSI}, which are shown in Table I along with the corresponding values in vacuum QED. This highlights the exotic nature of the eQED in QSI: the emergent photon travels 100×10^6 times slower than the speed of light and the emergent fine structure constant is ten times larger than its vacuum QED counterpart. The largeness of α_{QSI} implies substantial interactions between spinons and emergent photons in QSI, consistent with deviations from noninteracting theory expectations for the dynamic structure factor observed in quantum Monte Carlo at finite temperature [28].

The experimental effort to establish that these candidate materials realize the deconfined eQED phase at low temperature have largely been focused on finding evidence for the existence of a linearly dispersing transverse photon and fractionalized gapped spinons—the noninteracting structure of the emergent particles. However, the size of α_{QSI} suggest that distinctive experimental signatures may actually follow from the interaction effects between the particles. For example, due to α_{QSI}, we expect the dynamic structure factor observed in neutron scattering to exhibit the presence of well-defined spinon-antispinon "Rydberg" bound states, a strong Sommerfeld enhancement of the pair-production continuum at small momenta, and a strong diffusive suppression of the continuum at large momenta

due to emergent Cerenkov radiation within the sample [42]. Observation of such effects would thus constitute strong evidence for the eQED phase in these materials. The values of the constants determined here are inputs for quantitative comparison between theory and such experiments.

Finally, we note that our results make QSI a particularly attractive target for noisy intermediate-scale quantum simulations [43] of strongly coupled, deconfined QED in other experimental platforms. The microscopic construction requires only one two-level qubit per lattice link coupled by two-body local interactions; there have accordingly been detailed engineering proposals in, for example, ultracold Rydberg atoms [44], and demonstrations of closely related 2D ice in superconducting annealers [34]. The Schwinger model of $(1+1)$ D QED has in fact been realized in multiple quantum simulators recently [45,46]; however, it only exists in the confined phase. Our results show that the simple 3NN term (ζ) provides a direct tuning parameter for the emergent fine structure constant over a broad range to the strongest available coupling, allowing the controlled experimental investigation of strong coupling QED phenomena in $(3+1)$D. By varying ζ in space or time, this also gives a natural setting for studying the consequences of a space-time dependent fine structure constant—which contrasts with the usual QED where a large amount of effort concludes no such variation exists [47]. By varying the temperature and the corresponding density of emergent matter excitations, this further provides a platform for studying the behavior of strongly coupled plasma containing both electric charges and magnetic monopoles.

Originally introduced by Sommerfeld [48] to describe the fine structure of the spectral lines in hydrogen, the smallness of the fine structure constant $\alpha \sim 1/137$ has evolved into one of the great mysteries of our Universe. Its smallness enables the description of physical law in terms of weakly coupled matter and light, even as the largeness of $1/\alpha \sim 137$ determines the maximum stable atomic numbers of the periodic table and thus the richness of chemistry. However, despite almost a century of effort, there is no microscopic grand unified theory which predicts this fundamental parameter of our Universe. By studying the emergent phenomena provided by the strongly coupled eQED of spin ice, perhaps new light can be shed on this fundamental enigma.

The authors are grateful to Subhro Bhattacharjee, Anushya Chandran, Bert Halperin, and Frank Wilczek for discussions. We thank Boston University's Research Computing Services for their computational resources. S. D. P. acknowledges support from Boston University's Undergraduate Research Opportunities Program and from The Winston Churchill Foundation of the United States through the Churchill Scholarship. S. M. acknowledges funding from the Tsung-Dao Lee Institute. This work was in part supported by the Deutsche Forschungsgemeinschaft under Grants SFB 1143 (Project No. 247310070) and the cluster of excellence ct.qmat (EXC 2147, Project No. 390858490). C. R. L. acknowledges support from the NSF through Grant No. PHY-1752727. The authors wish to acknowledge the generous hospitality of the Galileo Galilei Institute for Theoretical Physics where this work was initiated and from the Aspen Center for Physics, which is supported by NSF Grant No. PHY-1607611.

[1] K. von Klitzing, in *Nobel Lectures in Physics 1981–1990*, edited by G. Ekspong (World Scientific Publishing Co., Singapore, 1993), pp. 309–346.
[2] G. Gabrielse, D. Hanneke, T. Kinoshita, M. Nio, and B. Odom, Phys. Rev. Lett. **97**, 030802 (2006).
[3] M. A. Levin and X.-G. Wen, Rev. Mod. Phys. **77**, 871 (2005).
[4] P. W. Anderson, Science **177**, 393 (1972).
[5] X.-G. Wen, Phys. Rev. Lett. **88**, 011602 (2001).
[6] O. I. Motrunich and T. Senthil, Phys. Rev. Lett. **89**, 277004 (2002).
[7] R. Moessner and S. L. Sondhi, Phys. Rev. B **68**, 184512 (2003).
[8] M. Hermele, M. P. A. Fisher, and L. Balents, Phys. Rev. B **69**, 064404 (2004).
[9] M. J. Gingras and P. A. McClarty, Rep. Prog. Phys. **77**, 056501 (2014).
[10] L. Pan, N. Laurita, K. A. Ross, B. D. Gaulin, and N. Armitage, Nat. Phys. **12**, 361 (2016).
[11] R. Sibille, N. Gauthier, H. Yan, M. C. Hatnean, J. Ollivier, B. Winn, U. Filges, G. Balakrishnan, M. Kenzelmann, N. Shannon, and T. Fennell, Nat. Phys. **14**, 711 (2018).
[12] J. Gaudet, E. M. Smith, J. Dudemaine, J. Beare, C. R. C. Buhariwalla, N. P. Butch, M. B. Stone, A. I. Kolesnikov, G. Xu, D. R. Yahne, K. A. Ross, C. A. Marjerrison, J. D. Garrett, G. M. Luke, A. D. Bianchi, B. D. Gaulin, Phys. Rev. Lett. **122**, 187201 (2019).
[13] B. Gao *et al.*, Nat. Phys. **15**, 1052 (2019).
[14] The terminology for the excitations in QSI differs among communities [9];we adopt the language used by the gauge theory literature where the spinon is called an electric charge. Our electric charge is referred to as a magnetic monopole in the classical spin ice literature and a spinon in the quantum spin liquid literature. Our magnetic monopole is also sometimes referred to as a vison in the quantum spin ice literature.
[15] J. B. Kogut, Rev. Mod. Phys. **51**, 659 (1979).
[16] A. Banerjee, S. V. Isakov, K. Damle, and Y. B. Kim, Phys. Rev. Lett. **100**, 047208 (2008).
[17] N. Shannon, O. Sikora, F. Pollmann, K. Penc, and P. Fulde, Phys. Rev. Lett. **108**, 067204 (2012).
[18] O. Benton, O. Sikora, and N. Shannon, Phys. Rev. B **86**, 075154 (2012).
[19] Y. Kato and S. Onoda, Phys. Rev. Lett. **115**, 077202 (2015).
[20] A. Szabó and C. Castelnovo, Phys. Rev. B **100**, 014417 (2019).
[21] M. P. Kwasigroch, Phys. Rev. B **102**, 125113 (2020).
[22] J. L. Cardy, Nucl. Phys. **B170**, 369 (1980).
[23] J. Luck, Nucl. Phys. **B210**, 111 (1982).

[24] G. Cella, U. M. Heller, V. K. Mitrjushkin, and A. Viceré, Phys. Rev. D **56**, 3896 (1997).
[25] S. T. Bramwell and M. J. Gingras, Science **294**, 1495 (2001).
[26] P. W. Anderson, Phys. Rev. **102**, 1008 (1956).
[27] C. Castelnovo, R. Moessner, and S. L. Sondhi, Annu. Rev. Condens. Matter Phys. **3**, 35 (2012).
[28] C.-J. Huang, Y. Deng, Y. Wan, and Z. Y. Meng, Phys. Rev. Lett. **120**, 167202 (2018).
[29] K. A. Ross, L. Savary, B. D. Gaulin, and L. Balents, Phys. Rev. X **1**, 021002 (2011).
[30] L. Savary and L. Balents, Phys. Rev. Lett. **108**, 037202 (2012).
[31] S. B. Lee, S. Onoda, and L. Balents, Phys. Rev. B **86**, 104412 (2012).
[32] J. G. Rau and M. J. Gingras, Annu. Rev. Condens. Matter Phys. **10**, 357 (2019).
[33] R. Moessner and K. S. Raman, in *Introduction to Frustrated Magnetism* (Springer, New York, 2011), pp. 437–479.
[34] A. D. King, C. Nisoli, E. D. Dahl, G. Poulin-Lamarre, and A. Lopez-Bezanilla, Science **373**, 576 (2021).
[35] H. Bernien, S. Schwartz, A. Keesling, H. Levine, A. Omran, H. Pichler, S. Choi, A. S. Zibrov, M. Endres, M. Greiner, V. Vuletić, and M. D. Lukin, Nature (London) **551**, 579 (2017).
[36] G. Pagano, A. Bapat, P. Becker, K. S. Collins, A. De, P. W. Hess, H. B. Kaplan, A. Kyprianidis, W. L. Tan, C. Baldwin, L. T. Brady, A. Deshpande, F. Liu, S. Jordan, A. V. Gorshkov, and C. Monroe, Proc. Natl. Acad. Sci. U.S.A. **117**, 25396 (2020).
[37] D. S. Rokhsar and S. A. Kivelson, Phys. Rev. Lett. **61**, 2376 (1988).
[38] See Supplemental Material at http://link.aps.org/supplemental/10.1103/PhysRevLett.127.117205 for (i) details on the exact diagonalization methods and structure of the constrained Hilbert space, (ii) the derivation of the coarse grained electromagnetic energy function and Gaussian photon dispersion, and (iii) details regarding the fit procedures and extrapolation methods.
[39] M. P. Kwasigroch, B. Douçot, and C. Castelnovo, Phys. Rev. B **95**, 134439 (2017).
[40] J. Jersák, T. Neuhaus, and P. M. Zerwas, Phys. Lett. B **133**, 103 (1983).
[41] J. S. Gardner, M. J. P. Gingras, and J. E. Greedan, Rev. Mod. Phys. **82**, 53 (2010).
[42] S. C. Morampudi, F. Wilczek, and C. R. Laumann, Phys. Rev. Lett. **124**, 097204 (2020).
[43] J. Preskill, Quantum **2**, 79 (2018).
[44] A. W. Glaetzle, M. Dalmonte, R. Nath, I. Rousochatzakis, R. Moessner, and P. Zoller, Phys. Rev. X **4**, 041037 (2014).
[45] E. A. Martinez, C. A. Muschik, P. Schindler, D. Nigg, A. Erhard, M. Heyl, P. Hauke, M. Dalmonte, T. Monz, P. Zoller, and R. Blatt, Nature (London) **534**, 516 (2016).
[46] B. Yang, H. Sun, R. Ott, H.-Y. Wang, T. V. Zache, J. C. Halimeh, Z.-S. Yuan, P. Hauke, and J.-W. Pan, Nature (London) **587**, 392 (2020).
[47] M. R. Wilczynska, J. K. Webb, M. Bainbridge, J. D. Barrow, S. E. Bosman, R. F. Carswell, M. P. Dąbrowski, V. Dumont, C.-C. Lee, A. C. Leite, A. C. Leite, K. Leszczyńska, J. Liske, K. Marosek, C. J. A. P. Martins, D. Milaković, P. Molaro, and L. Pasquini, Sci. Adv. **6**, eaay9672 (2020).
[48] A. Sommerfeld, Ann. Phys. (N.Y.) **356**, 1 (1916).